High Molar Extinction Coefficient Heteroleptic Ruthenium Complexes for Thin Film Dye-Sensitized Solar Cells

ARTICLE *in* JOURNAL OF THE AMERICAN CHEMICAL SOCIETY · APRIL 2006

Impact Factor: 12.11 · DOI: 10.1021/ja058540p · Source: PubMed

8 AUTHORS, INCLUDING:

Dai-Bin Kuang
Sun Yat-Sen University
111 PUBLICATIONS **5,821** CITATIONS
SEE PROFILE

Seigo Ito
University of Hyogo
106 PUBLICATIONS **10,672** CITATIONS
SEE PROFILE

Bernard Wenger
University of Oxford
22 PUBLICATIONS **1,135** CITATIONS
SEE PROFILE

Jacques-E. Moser
École Polytechnique Fédérale de Lausanne
170 PUBLICATIONS **16,394** CITATIONS
SEE PROFILE

FULL PAPER

ADVANCED FUNCTIONAL MATERIALS

DOI: 10.1002/adfm.200600483

High Molar Extinction Coefficient Ion-Coordinating Ruthenium Sensitizer for Efficient and Stable Mesoscopic Dye-Sensitized Solar Cells**

By *Daibin Kuang*, *Cedric Klein*, *Seigo Ito*, *Jacques-E. Moser*, *Robin Humphry-Baker*, *Shaik. M. Zakeeruddin*,* and *Michael Grätzel**

Ru(4,4-dicarboxylic acid-2,2′-bipyridine) (4,4′-bis(2-(4-(1,4,7,10-tetraoxyundecyl)phenyl)ethenyl)-2,2′-bipyridine) $(NCS)_2$, a new high molar extinction coefficient ion-coordinating ruthenium sensitizer was synthesized and characterized using ^{1}H NMR, Fourier transform IR (FTIR), and UV/vis spectroscopies and cyclic voltammetry. Using this sensitizer in combination with a nonvolatile organic-solvent-based electrolyte, we obtain a photovoltaic efficiency of 8.4 % under standard global AM 1.5 sunlight. These devices exhibit excellent stability when subjected to continuous thermal stress at 80 °C or light soaking at 60 °C for 1000 h. An electrochemical impedance spectroscopy study revealed that device stability is maintained by stabilizing the TiO_2/dye/electrolyte and Pt/electrolyte interface during the aging process. The influence of Li^+ present in the electrolyte on the device photovoltaic parameters was studied, and the FTIR spectral and photovoltage transient study showed that Li^+ coordinates to the triethyleneoxide methylether side chains on the K60 sensitizer molecules.

1. Introduction

Mesoscopic dye-sensitized solar cells (DSCs) have been attracting intensive interest for scientific research and industrial applications because of their high photon-to-electricity conversion efficiency and low cost compared with traditional photoelectrochemical cells.[1,2] Since the discovery of DSCs, impressive improvements have been achieved on the photovoltaic performance and the stability of devices.[2] To increase the photovoltaic performance of the DSCs, much effort has been paid to the development of sensitizer, electrolyte, and photoanode materials.[3–7] Although a variety of sensitizers, including metal-free organic dyes and non-ruthenium metal dyes have been used, ruthenium polypyridine complexes exhibit the best performance to date.[8–10]

Recently, we introduced a new class of heteroleptic ruthenium complexes endowed with a bipyridine ligand that is substituted by two triethyleneoxide methyl ether (TEOME) groups instead of the two nonyl chains of the Z907 dye.[5] The higher photocurrent and performance for K51 compared with Z907 was attributed to much-faster dye regeneration in the former case.[5] However, the two drawbacks of K51 are its low molar extinction coefficient and its high solubility in organic solvents, which are caused by the hydrophilic TEOME groups. The dye desorption into the electrolyte renders the stability of devices based on K51 poor at 80 °C. As reported in our earlier publications,[4,11] extending the π-conjugation of the ligand enhances the extinction coefficient of the sensitizer and also decreases its solubility impairing dye desorption. Thus, in this paper, we report on the synthesis of a K60 dye incorporating both the extended π-conjugation and the ion-coordinating TEOME group. The photovoltaic performance of the K60 dye in combination with the nonvolatile organic electrolyte and the Li^+ coordinating capability of this sensitizer was monitored using FTIR spectral studies.

2. Results and Discussion

The molecular structure of K60 dye is shown in Figure 1 and synthetic details are given in the Experimental section.

2.1. Attenuated Total Reflection Fourier Transform IR (ATR-FTIR)

Structural information on the configuration of K60 adsorbed onto the TiO_2 surface was derived from ATR-FTIR spectroscopy results.[12] Figure 2 shows the ATR-FTIR spectrum of the K60 dye anchored on the mesoscopic TiO_2 film surface, corrected by subtracting a spectrum of a TiO_2 reference film heated to 500 °C. The strong signal peak at 2102 cm^{-1} is attributed to the N-coordinated thiocyanate group (ν(CN)). The peak at 1382 cm^{-1} and the underlying peak at 1596 cm^{-1} arise

[*] Dr. S. M. Zakeeruddin, Prof. M. Grätzel, Dr. D. Kuang, Dr. C. Klein, Dr. S. Ito, Prof. J.-E. Moser, Dr. R. Humphry-Baker
Laboratory for Photonics and Interfaces
Institute of Chemical Sciences and Engineering
Ecole Polytechnique Fédérale de Lausanne
1015 Lausanne (Switzerland)
E-mail: shaik.zakeer@epfl.ch; michael.graetzel@epfl.ch

[**] We are grateful to P. Comte and R. Charvet for the nanocrystalline TiO_2 paste fabrication, T. Koyanagi (CCIC, Japan) for providing the 400 nm sized TiO_2 particles. The Swiss Science Foundation and Swiss Federal Office for Energy (OFEN) have supported this work.

ADVANCED FUNCTIONAL MATERIALS

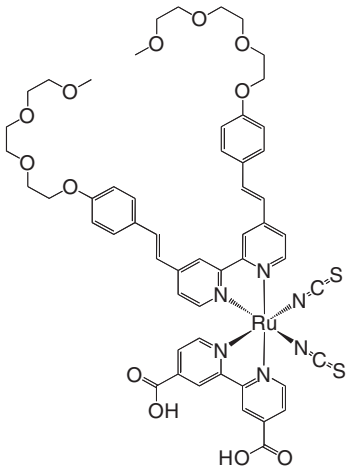

Figure 1. The molecular structure of the K60 sensitizer.

from the symmetric and asymmetric stretching modes of carboxylate groups ($\nu(COO^-)$), respectively. The sharp peak located at 1538 cm^{-1} is ascribed to bipyridyl modes, while the sharp peak at 1596 cm^{-1} is due to the styryl bond. The peaks observed at 2875 and 2919(sh) cm^{-1} are due to the symmetric and asymmetric stretching modes of the CH_2 units of the ethylene oxide chains, respectively. The medium broad peak at 1116 cm^{-1} is derived from the ν(C–O) stretch of the polyethylene oxide group. The broadness of the latter peak signifies the disordered nature of these chains.

The coordination ability of K60 sensitizer with Li^+ was further investigated by using FTIR. The K60 dye adsorbed on the surface of a TiO_2 film was exposed to a 0.25 M lithium iodide in acetonitrile solution, and changes in the IR spectrum of K60 were monitored. In the region of the ν(C–O) stretch at 1116 cm^{-1} there is a shift to lower energy, which is caused by coordination with lithium ions. This difference is shown in the inset of Figure 2. The peak appearing at 1084 cm^{-1} is due to C–O···Li^+ coordination, which lowers the frequency of the C–O vibration.[5,13] The peak at 1036 cm^{-1} is due to the acetonitrile solvent, which presumably interpenetrates into the dye/TiO_2 interface. Since the Li^+ free ν(C–O) peak is diminished approximately by 50 % in the presence of Li^+, an average of one Li^+ is associated with each dye under these conditions. Upon rinsing the film with pure acetonitrile, the original peaks are restored.

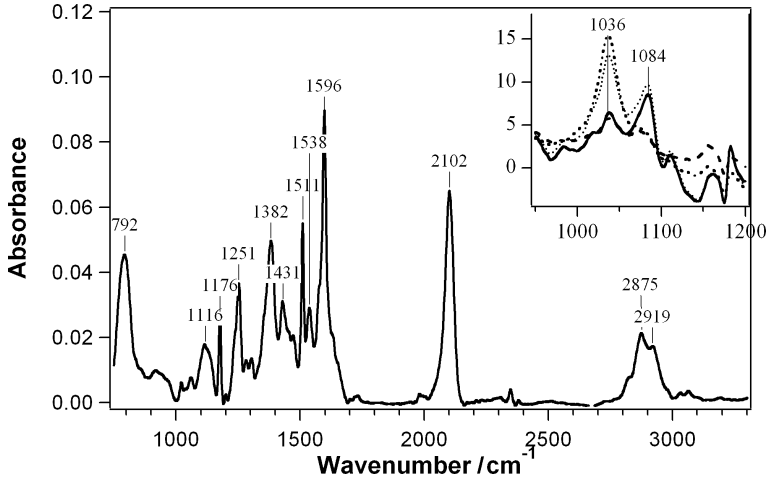

Figure 2. The ATR-FTIR spectrum of the K60 dye adsorbed on a 6 μm thick mesoscopic TiO_2 film. The spectrum from a TiO_2 reference film heated to 500 °C has been subtracted. The inset shows the difference spectra after the addition of 0.25 M lithium iodide in acetonitrile solution. The solid curve is immediately after addition and the dot dashed after 5 min. The dashed line is obtained after washing with pure acetonitrile.

2.2. Absorption and Luminescence Spectroscopy

Figure 3 presents the UV-vis absorption and emission spectrum of the K60 dye in dimethylformamide (DMF) solution. The absorption spectra shows the lowest metal-to-ligand charge transfer (MLCT) absorption band at 547 nm with a molar extinction coefficient of 18.55×10^3 M^{-1} cm^{-1}. The absorption bands at 356 and 310 nm correspond to the π–π* transitions of 4,4′-bis(2-(4-(1,4,7,10-tetraoxyundecyl)phenyl)ethenyl)-2,2′-bipyridine and 4,4′-dicarboxylic acid 2,2′-bipyridine, respectively. The luminescence maximum is located at 825 nm. Based on both the absorption and emission spectra, the E_{0-0} transition energy of the dye was estimated to be 1.7 eV. The standard potential ($\phi^0(S^+/S^*)$) of the K60 can be calculated from the relation $\phi^0(S^+/S) = \phi^0(S^+/S^*) - E_{0-0}$, yielding –0.69 V versus the normal hydrogen electrode (NHE). So, $\phi^0(S^+/S^*)$ of K60 is more negative (or higher in energy) than the conduction band edge of TiO_2, providing a thermodynamic driving force of electron injection from the dye to TiO_2.

2.3. Redox Behavior of the K60 Dye

The typical cyclic voltammetry (CV) result of the K60 dye anchored on 6 μm thick mesoscopic TiO_2 is shown in Figure 4. A reversible redox wave centered at 1.01 V versus NHE is observed, which is 0.5 eV more positive than the potential of the iodide/triiodide redox couple in the electrolyte, providing a large thermodynamic driving force for regeneration of the K60 dye by iodide.

2.4. Kinetics of Electron-Transfer Processes

The excited-state lifetime of K60 was determined by using nanosecond transient absorbance spectroscopy. The dye was adsorbed on a transparent nanocrystalline alumina film, covered by aerated 3-methoxypropionitrile as solvent. The high-energy-lying conduction band of alumina is out of reach for the K60 excited state, and no charge injection occurs in this case. The decay of the dye excited-state absorption signal was monitored at $\lambda = 620$ nm and yielded a lifetime $\tau = (13.2 \pm 0.5)$ ns. Electron injection from photoexcited Ru^{II} polypyrridyl sensitizers into the conduction band of TiO_2 takes place typically in the femtosecond–picosecond time frame.[4,14,15] Hence, the natural decay of the excited state of K60 cannot compete kinetically with the interfacial charge-trans-

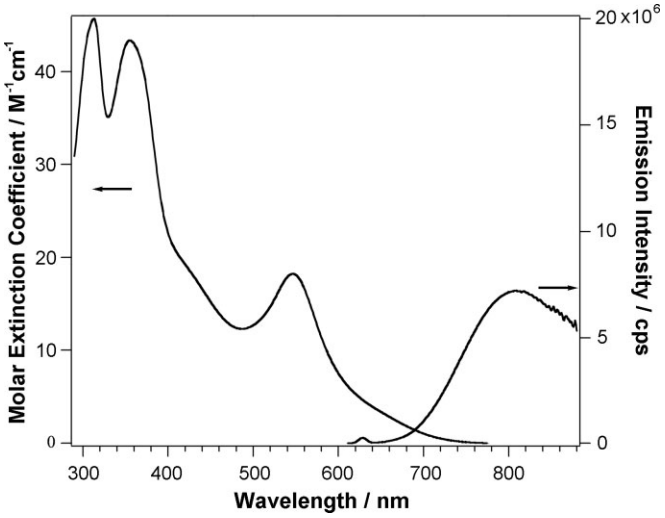

Figure 3. Electronic absorption and emission spectra of the K60 dye in DMF solution.

fer process. Thus, quantitative electron injection into the K60-sensitized TiO_2 electrode upon illumination is expected.

The photovoltaic performance of DSCs is largely dependent of the kinetic competition between back electron transfer from the conduction band of the semiconductor electrode to the oxidized dye cations (S^+) and the interception of the oxidized sensitizer by the redox mediator. Nanosecond laser transient absorbance measurements were performed to scrutinize the kinetics of these two charge-transfer processes for the K60 dye. Great care was taken to keep the excitation laser pulse intensity as low as possible (fluence $< 20\ \mu J\,cm^{-2}$) in order to ensure that at most one electron was injected at a time per TiO_2 nanoparticle. Also, the probe light intensity was reduced to a minimum using filters and a monochromator before the sample, to avoid light biasing of the sensitized TiO_2 films. In a ruthenium(III) polypyridyl complex containing thiocyanate ligands, the oxidized state (S^+) has a characteristic absorption at $\lambda > 620$ nm that is due to a ligand-to-metal charge-transfer (LMCT) transition. In the absence of a redox mediator (pure 3-methoxypropionitrile solvent), the decay of the absorption signal recorded at $\lambda = 680$ nm reflects the dynamics of the recombination of injected electrons with the oxidized dye (S^+). Figure 5 shows that the transient absorbance of the oxidized state of the K60 dye decays with a typical half-reaction time $t_{1/2} = 200$ μs. The charge-recombination kinetics for K60 is comparable to that of the K51 sensitizer in 3-methoxypropionitrile (MPN) solvent ($t_{1/2} = 200$ μs).[5] In the presence of the iodide/triiodide redox couple the decay of the oxidized-dye signal was significantly accelerated with the half-reaction time decreasing to $t_{1/2} = 10$ μs. The regenaration rate was similar to that reported earlier for K51.[5] It shows the charge-recombination process from the oxidized-dye state is indeed intercepted by the mediator, and the sensitizer efficiently regenerated by iodide ($S^+ \,|\, TiO_2 + D \rightarrow S \,|\, TiO_2 + D^+$).

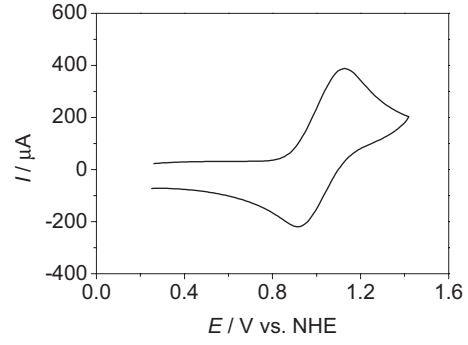

Figure 4. CV of the K60 dye adsorbed on a 6 μm thick transparent nanocrystalline TiO_2 electrode; scan rate is 100 mV s^{-1}. The electrolyte is 0.1 M tetrabutylammonium perchlorate in acetonitrile.

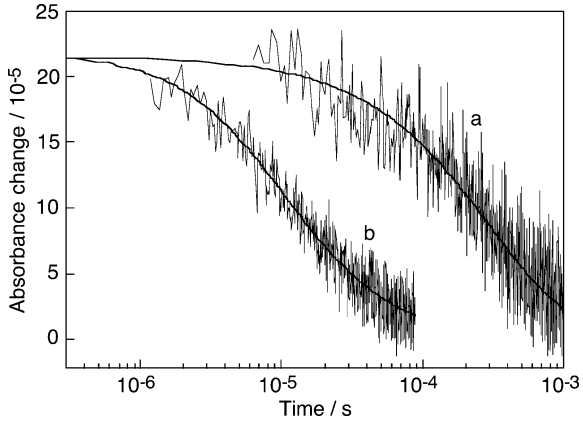

Figure 5. Transient absorbance decay kinetics of the oxidized state of K60 dye adsorbed on nanocrystalline TiO_2 films in pure 3-methoxypropionitrile (a), and in the presence of a iodide/triiodide redox couple nonvolatile electrolyte (b). Absorbance changes were measured at a probe wavelength of 680 nm upon 600 nm pulsed laser excitation (5 ns full width at half-maximum pulse duration, 15 μJ cm^{-2} pulse fluence, 30 Hz repetition rate). Signals as shown were obtained by typically averaging over 3000 individual traces.

2.5. Photovoltaic Performance

Figure 6a presents the photocurrent density–voltage curve of the device with K60 dye alone (device A) or in the presence of 1-decylphosphonic acid (DPA) as a coadsorbent (device B) under AM 1.5 simulated sunlight at a light intensity of 100 mW cm^{-2}. The short-circuit current density (J_{sc}), open-circuit voltage (V_{oc}), fill factor (FF) and overall conversion efficiency (η) of device A are 16.0 mA cm^{-2}, 725 mV, 0.68 and 8.02 %, respectively. For device B the photovoltaic parameters are 16.7 mA cm^{-2}, 735 mV, 0.69 and 8.44 %, respectively. At one third of a solar light intensity (30 mW cm^{-2}), the power conversion efficiency exceeded even 9.0 %. The detailed photovoltaic parameters for devices A and B under different light irradiance are shown in Table 1. The overall power conversion efficiency of devices with DPA coadsorbent increases (from 8.0 to 8.44 %) mainly because of the increase in the J_{sc} and V_{oc} (Fig. 6a and Table 1). The mixed monolayer K60–DPA may impair the back electron transfer from the conduction band or surface state of TiO_2 to the triiodide in the electrolyte,

ADVANCED FUNCTIONAL MATERIALS

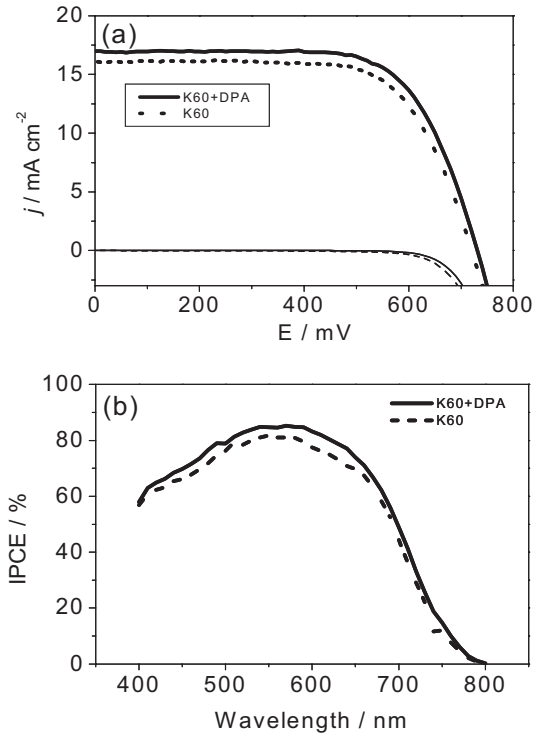

Figure 6. a) Photocurrent density (*j*)–voltage (*E*) characteristics of a DSC device based on a K60 sensitizer in the absence (device A) or presence (device B) of DPA coadsorbent and nonvolatile electrolyte, measured at air mass 1.5 (AM 1.5, 100 mW cm^{-2}) full sunlight illumination. b) Photocurrent action spectrum of devices A and B.

which may be the reason for the increase in the J_{sc} and V_{oc} values.[3]

The incident photo-to-current conversion efficiency (IPCE) for devices A and B are compared in Figure 6b. For device B it exceeds 80 % in the spectral range 480–650 nm, reaching its maximum of 85 % at 540 nm, which is higher than that of device A, explaining its superior performance.

Figure 7 presents the variation in the photovoltaic parameters at 80 °C in the dark with aging time for device B. The photocurrent decreased by 7 % while the V_{oc} dropped by 30 mV, which was compensated for by a 5 % increase in the *FF*, during 1000 h of aging at 80 °C. Thus, the device showed excellent stability by maintaining 94 % of its initial photovoltaic performance. Furthermore, in the absence of DPA as a coadsorbent, device A also exhibited good thermal stability. It is interesting to note that in the absence of DPA the devices showed stable photocurrents, whereas the devices with DPA maintained a relatively stable photovoltage. Thus, DPA coadsorption was found to stabilize the photovoltage because of the formation of a robust and compact molecular monolayer at the mesoscopic TiO_2 surface and to the exclusion of water from the interface of TiO_2, stabilizing the quasi-Fermi level of the semiconductor electrode.[3,16] To investigate the photostability, the devices covered with a 50 μm thick polymer as a UV cutoff filter (up to 400 nm) were irradiated by 100 mW cm^{-2} of simulated solar light at 60 °C for 1000 h under a Suntest CPS plus lamp. Both devices A and B retained more than 93 % of their initial performance after aging for 1000 h.

Table 1. Detailed photovoltaic parameters of devices A and B under different sunlight irradiation [a].

	Light intensity	J_{SC} [mA cm^{-2}]	V_{OC} [mV]	*FF*	η [%]
	1.0 sun	16.28	720.49	0.684	8.02
A	0.52 sun	8.79	703.49	0.734	8.56
	0.3 sun	5.2	688.13	0.740	8.69
	1.0 sun	16.85	730.09	0.686	8.44
B	0.52 sun	9.23	714.51	0.734	9.10
	0.3 sun	5.29	700.13	0.755	9.21

[a] The spectral distribution of the Xenon lamp simulates AM 1.5 solar light. 1.0 sun was mismatch corrected to correspond to AM 1.5 global sunlight (100 mW cm^{-2}). The cell active areas were 0.158 cm^{-2}.

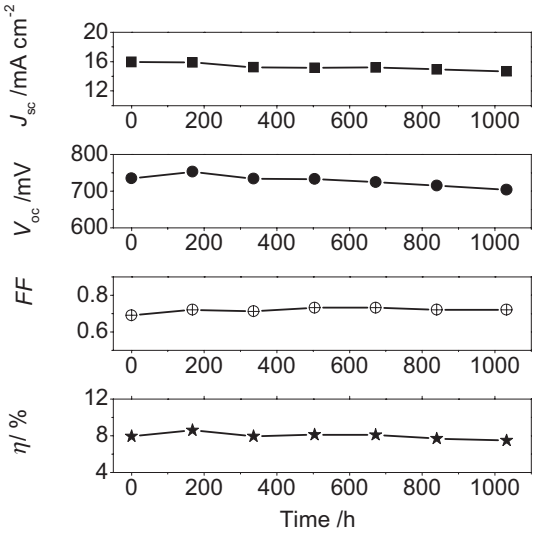

Figure 7. Variations in photovoltaic parameters (J_{sc}, V_{oc}, *FF*, and η) with aging time for the device based on K60–DPA and nonvolatile electrolyte during successive aging at 80 °C in the dark.

2.6. Electrochemical Impedance Spectroscopy (EIS) Studies

Recent studies have shown that EIS is a useful technique to reveal the variations in the DSCs system performance during long-term aging.[17–21] A freshly prepared device (B) was aged at 80 °C for 1000 h, and analyzed under 1 sun illumination at open circuit. These measurements showed three semicircles in the Nyquist diagram (Fig. 8a) or three characteristic frequency peaks in Bode phase plots (Fig. 8b). In Figure 8b, in order of increasing frequency, the three frequency peaks correspond to Nernst diffusion in the electrolyte, recapture of electrons from the conduction band of TiO_2 by the I_3^- interface as well as electron transport in TiO_2 film, and redox charge transfer at the counter electrode, respectively.

The characteristic middle peak shifted to a higher value after aging for 1000 h at 80 °C according to the Bode phase plots (Fig. 8b), revealing a decrease in the electron-recombination time (τ) from 19.1 to 7.4 ms. This implies that the photovoltage decreases because of a decreasing electron lifetime, which is consistent with the above photovoltaic data. The high-fre-

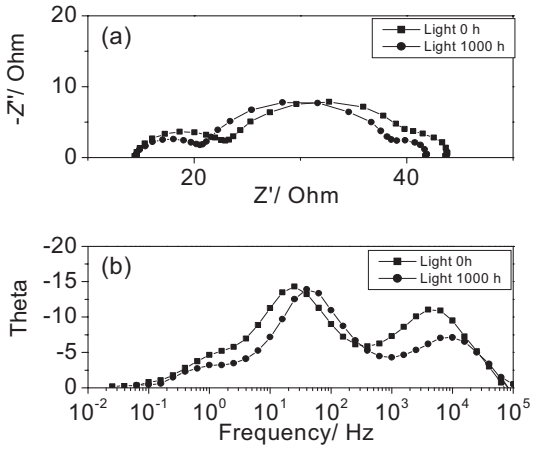

Figure 8. Impedance spectra of DSC devices based on K60–DPA and nonvolatile electrolyte for a fresh cell and an aged (after 1000 h at 80 °C) cell, measured at 1 sun illumination at open-circuit potential. a) Nyquist plots. b) Bode phase plots.

quency peak corresponding to electron transfer on the counter electrode ($I_3^- + 2e = 3I^-$) also shifts to a higher frequency for aged cells. This reveals that the increase in *FF* arises from faster electron transfer at the counter electrode. Thus, the shift of the characteristic peaks at middle and high frequencies can reasonably explain the observed photovoltaic data variation with aging time, namely, decrease in the photovoltage of ca. 30 mV and an increase of ca. 5 % in the *FF*.

2.7. Influence of Li^+ on the Photovoltaic Performance

Furthermore, we investigated the effect of Li^+ in the present nonvolatile organic-solvent electrolyte on the photovoltaic parameters of the DSC with a K60 sensitizer. With 50 mM $LiClO_4$ in the electrolyte, the photovoltage dropped 27 mV, accompanied by an increase in the current, as shown in Figure 9. This may be due to the Li^+ coordination with the TEOME group of the K60 sensitizer, preventing most of the Li^+ from coordinating to the TiO_2 surface. Thus, the conduction band level of mesoscopic TiO_2 is not expected to shift. However, for a non-

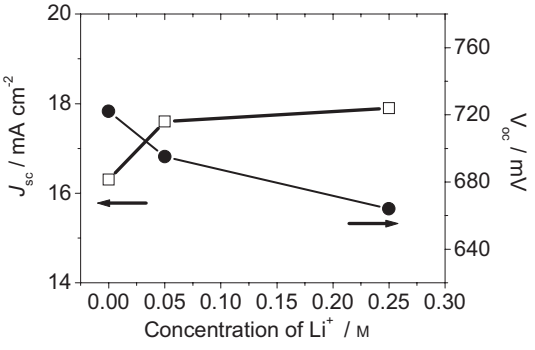

Figure 9. The variations in J_{sc} and V_{oc} of DSC devices made with a K60 dye with nonvolatile organic-solvent electrolyte containing different Li^+ concentrations.

ion-coordinating sensitizer, Z907Na, the drop in photovoltage is observed to be 50 mV. When the concentration of $LiClO_4$ increased to 0.25 M in the electrolyte, we found a 58 mV drop in photovoltage for the K60 sensitizer. This is because most of the coordinating capacity of the K60 sensitizer has been exceeded and Li^+ remains free to adsorb to the TiO_2 surface lowering the conduction-band level and hence the V_{oc}. The influence of Li^+ on the J_{sc} and V_{oc} for the K60 sensitizer is very similar to the one previously observed with the K51 dye.[5]

Surface adsorption of Li ion has an influence on the charge-recombination rate and the position of the quasi-Fermi level. To explore the consequences of Li-ion adsorbed to the surface it would be useful to determine charge-recombination rates. Using the transient-voltage-decay technique, the voltage-response time for the reaction of the injected charge and the mediator was monitored for electrolytes containing different Li-ion concentrations.

In the absence of Li ions, a response time of typically 5 ms was found for K60. Addition of 50 mM Li had only a small impact on this lifetime but for the 250 mM Li-containing electrolyte, the lifetime was in excess of 8 ms. This is clearly consistent with a slower recombination process leading to a high J_{sc}. The experiment repeated with Z907Na as the sensitizer, which does not contain the ion-coordination functionality, shows a 2-fold change in the transient response lifetime in the presence of only 50 mM Li ions (from 5.5 ms to 10.4 ms). These results show clearly the implication of the Li-ion coordination on the K60 sensitizer.

3. Conclusions

A new high molar extinction coefficient ion-coordinating sensitizer was synthesized. With this new sensitizer (K60), photovoltaic power conversion efficiency of 8.4 % under AM 1.5 simulated sunlight at a light intensity of 100 mW cm^{-2} has been obtained based on nonvolatility organic-solvent electrolyte. Photovoltaic performance greater than 9 % was reached under low light irradiance (30 mW cm^{-2}). The DSC devices showed excellent stability when submitted to long-term high-temperature stress and light-soaking tests. The DSC devices maintains more than 93 % of the initial photovoltaic performance after aging at 80 °C in the dark or 60 °C under visible-light soaking (simulated sun light: 100 mW cm^{-2}) for 1000 h. The EIS study revealed that during the aging process the interface of the TiO_2/dye/electrolyte and Pt/electrolyte exhibit good stability for excellent performance. FTIR and photovoltage transient studies proved the coordination ability of the K60 sensitizer with Li^+.

4. Experimental

4.1. Reagents and Materials Synthesis

Reagents: A new ion-coordinating high molar extinction coefficient sensitizer, Ru(4,4-dicarboxylic acid-2,2′-bipyridine) (4,4′-bis(2-(4-(1,4,7,10-tetraoxyundecyl)phenyl)ethenyl)-2,2′-bipyridine) $(NCS)_2$ was

synthesized according to Scheme 1. The molecular structure of K60 is shown in Figure 1. Guanidinium thiocyanate (GuNCS) purchased from Fluka and DPA from Lancaster were used as received. *N*-Methylbenzimidazole (NMBI, from Aldrich) was recrystallized from diethyl ether before use. 4-(1,4,7,10-Tetraoxyundecyl)benzaldehyde was synthesized according to the reported literature procedure [22].

4,4′-Bis(2-(4-(1,4,7,10-tetraoxyundecyl)phenyl)ethenyl)-2,2′-bipyridine (L): Solid *t*-BuOK (1.5 g, 13.4 mmol) was added to a solution of 4,4′-bis(diethylmethylphosphonate)-2,2′-bipyridine (1.5 g, 3.3 mmol) and 4-(1,4,7,10-tetraoxyundecyl)benzaldehyde (2.1 g, 7.8 mmol) in dry tetrahydrofuran (THF, 150 mL). The resulting mixture was stirred overnight at room temperature under nitrogen. The slurry was then filtered over Celite and the filter cake washed with THF and CH_2Cl_2. The filtrate was evaporated until dry, and the resulting residue was dissolved in a minimum of CH_2Cl_2 and Et_2O was added. The formed precipitate was filtered off and washed with Et_2O to afford 1.8 g (80 %) of the titled compound (L) as a white solid. ^{1}H NMR (200 MHz, 25 °C, $CDCl_3$) δ [ppm]: 3.39 (s, 6H), 3.5–3.7 (m, 16H), 3.88 (t, J = 4.5 Hz, 4H), 4.18 (t, J = 4.5 Hz, 4H), 6.94 (d, J = 8 Hz, 4H), 7.00 (d, J = 16 Hz, 2H), 7.4–7.5 (m, 8H), 8.52 (s, 2H), 8.65 (d, J = 5 Hz, 2H). ^{13}C NMR (50 MHz, 25 °C, $CDCl_3$) δ [ppm]: 59.0, 67.5, 69.7, 70.6, 70.7, 70.8, 71.9, 114.9, 118.0, 120.8, 124.0, 128.4, 129.2, 132.8, 146.1, 149.4, 156.5, 159.3.

Ru(L)(p-cymene)(Cl)$_2$: A mixture of L (0.85 g, 1.24 mmol) and $[Ru(Cl)_2(p\text{-cymene})]_2$ (0.38 g, 0.62 mmol) in EtOH (80 mL) was refluxed for 4 h under nitrogen. Evaporation of the solvent afforded the pure complex as an orange oil.

Ru(L)(L′)(NCS)$_2$: Ru(L)(*p*-cymene)$(Cl)_2$ and 4,4′-dicarboxy-2,2′-bipyridine, abbreviated as L′, (0.303 g, 1.24 mmol) in anhydrous DMF (60 mL) were heated to 140 °C for 4 h under nitrogen and in the dark. NH_4NCS (1.5 g, 19.7 mmol) was then added to the mixture and heating was continued for 4 h. After cooling to room temperature, DMF was evaporated and water (200 mL) was added. The resulting purple solid was filtered and washed with water. The crude complex was dissolved in basic methanol [with tetrabutylammonium hydroxide (TBAOH)] and further purified on a Sephadex LH 20 with methanol as eluent. The main band was collected, concentrated, and precipitated with dilute acedic methanol to obtain pure K60. ^{1}H NMR (200 MHz, 25 °C, CD_3OD+NaOD) δ [ppm]: 9.45 (d, 1H), 9.15 (d, 1H), 8.95 (s, 1H), 8.8 (s, 1H), 8.35 (s, 1H), 8.2 s, 1H), 8.0 (d, 1H), 6.7 to 7.9 (m, 17H), 4.4 to 1.0 (m, 48H). Analytical calculation for $RuC_{54}H_{55.5}N_6O_{12}S_2 \cdot 2\,H_2O \cdot 0.5\,(TBA)$: C, 57.2; H, 6.0; N, 7.0 %. Found; C, 57.9; H, 5.9; N, 7.1 %.

4.2. Measurements

UV-vis and photoluminescence spectra were measured in a 1 cm path-length quartz cell using a Cary 5 spectrophotometer or Spex Fluorolog 112 spectrofluorometer, respectively. The emitted light was detected with a Hamamatsu R2658 photomultiplier operated in single-photon counting mode. The emission spectrum was photometrically corrected with a calibrated 200 W tungsten lamp as a reference source. ^{1}H NMR measurements were carried out on a Bruker 200 MHz spectrometer. The ^{1}H spectra were referenced to tertramethylsilane.

FTIR Measurements: The ATR-FTIR spectrum of the K60 sensitizer was measured using a Digilab FTS 7000 FTIR spectrometer fitted with a deuterated triglycine sulfate (DTGS) detector. The data reported here was taken with the 'Golden Gate' 45° diamond anvil ATR accessory. Spectra were derived from 64 scans at a resolution of 2 cm^{-1}. Prior to measuring the spectra, the dyed films were rinsed with acetonitrile solvent to wash out any weakly adsorbed molecules and then dried.

Nanosecond Laser Transient Absorbance Measurements: Dye-coated, transparent nanocrystalline TiO_2 films 8 μm in thickness were excited by nanosecond laser pulses produced by a broad-band optical parametric oscillator (OPO GWU-355), pumped by a frequency-tripled Q-switched Nd:YAG (yttrium aluminum garnet) laser (Continuum Powerlite 7030). Excitation pulses (λ = 600 nm, 30 Hz repetition rate, pulse width at half-height of 7 ns) were attenuated by neutral density filters to reduce the pulse fluence on the sample down to 15 μJ cm^{-2}. The probe light from a Xe arc lamp was passed through a monochromator, various optical elements, the sample, and a second monochromator before being detected by a fast photomultiplier tube. Typically, averaging over 3000 laser shots was necessary to get satisfactory signal-to-noise levels.

Photovoltage transients were observed using an exciting pulse generated by a ring of red-light-emitting diodes (LEDs, Lumiled) controlled by a fast solid-state switch. Pulse widths of 200 ms were used. The pulse was incident on the photoanode side of the device, and its intensity was controlled to keep the modulation of the voltage below 5 mV. A white bias light, also incident on the same side of the device, was supplied by white diodes. Usually, transients were measured at different white-light intensities ranging from 150 to 0.1 % sun by tuning the applied voltage on the bias diodes.

EIS Measurements: Impedance spectra of the fresh and aged cell were measured under full-sun irradiance at open circuit using a potentiostat (EG&G, M273) equipped with a frequency response analyzer (EG&G, M1025). The spectra were scanned in a frequency range 0.005 Hz–100 KHz at room temperature with the alternating voltage amplitude set at 10 mV.

Electrochemical Measurements: Voltammetric measurements were recorded using a PC-controlled AutoLab PSTAT10 electrochemical workstation. Cyclic voltammograms of the K60 sensitizer adsorbed on 6 μm thick transparent TiO_2 were obtained using 0.1 M tetrabutylammonium perchlorate in acetonitrile as electrolyte.

Fabrication of DSC Devices: The photoanode of the DSC is a double-layer TiO_2 film containing a transparent layer 6.8 μm thick (20 nm nanoparticles) and a scattering layer of 4 μm thick (400 nm nanoparticles) [4]. The double-layer films were heated to 520 °C and sintered for 30 min, then cooled to ca. 80 °C and immersed into the dye solution at room temperature for 14 h. The dye solution containing 300 μM of K60

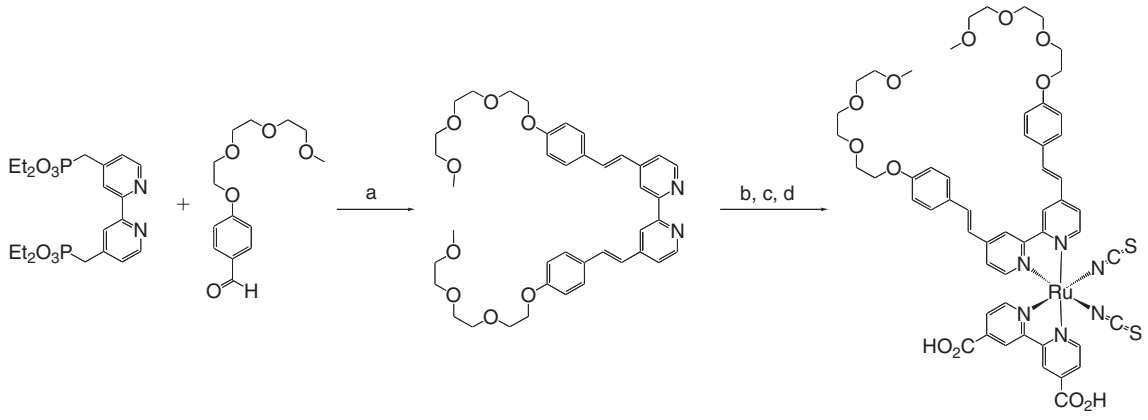

Scheme 1. a) *t*-BuOK, THF, 25 °C. b) $[Ru(Cl)_2(p\text{-cymene})]_2$, EtOH, Δ. c) 4,4′-dicarboxy-2,2′-bipyridine, DMF, 140 °C. d) NH_4NCS, DMF, 140 °C.

in acetonitrile and *tert*-butyl alcohol (volume ratio: 1:1) was used to sensitize the photoanode. In the presence of coadsorbent, 75 μM of DPA was added to the above dye solution. Dye-coated double-layer films were assembled and sealed with a thin (35 μm thick) transparent hot-melt Bynel ring (DuPont) to the counter electrodes (Pt on fluorine tin oxide glass, chemical deposition of 0.05 M hexachloroplatinic acid in isopropyl alcohol at 400 °C for 15 min). The electrolyte was injected into the interelectrode space from the counter-electrode side through a predrilled hole, and then the hole was sealed with a Bynel sheet and a thin-glass-slide cover by heating. The nonvolatile electrolyte contains 0.8 M 1-propyl-3-methylimidazolium iodide (PMII), 0.15 M iodine, 0.1 M GuNCS, and 0.5 M NMBI in 3-methoxypropionitrile.

Photocurrent–Voltage Measurements: The current–voltage curves were obtained by measuring the photocurrent of the cells using a Keithley model 2400 digital source meter (Keithley, USA) under an applied external potential scan. The irradiation source for the photocurrent–voltage (*I–V*) measurement is a 450 W xenon light source (Osram XBO 450, USA), which simulates the solar light. The measurement of the IPCE was performed by a similar data-collecting system but under monochromatic light. The incident light from a 300 W Xenon lamp (ILC Technology, USA) was focused through a Gemini 180 double monochromator (Jobin Yvon, UK) onto the cell under test.

Light-Soaking Stability: The cells were covered with a polymer film of 50 μm thickness (Preservation Equipment, UK), which acts as a UV cutoff filter and were illuminated at open circuit under a Suntest CPS lamp (ATLAS, 100 mW cm^{-2}, 60 °C). The cells were taken out at regular intervals to record the photocurrent–voltage curve measured over a period of 1000 h.

Received: June 2, 2006
Revised: August 30, 2006
Published online: November 24, 2006

[1] B. O'Regan, M. Grätzel, *Nature* **1991**, *353*, 737.
[2] a) M. Grätzel, *Nature* **2001**, *414*, 338. b) M. Grätzel, *Chem. Lett.* **2005**, *34*, 8.
[3] P. Wang, C. Klein, R. Humphry-Baker, S. M. Zakeeruddin, M. Grätzel, *Appl. Phys. Lett.* **2005**, *86*, 123 508.
[4] D. Kuang, S. Ito, B. Wenger, C. Klein, J.-E. Moser, R. Humphry-Baker, S. M. Zakeerudddin, M. Grätzel, *J. Am. Chem. Soc.* **2006**, *128*, 4146.
[5] D. Kuang, C. Klein, H. J. Snaith, J.-E. Moser, R. Humphry-Baker, P. Comte, S. M. Zakeeruddin, M. Grätzel, *Nano Lett.* **2006**, *6*, 769.
[6] a) F. Lenzmann, J. Krueger, S. Burnside, K. Brooks, M. Grätzel, D. Gal, S. Rühle, D. Cahen, *J. Phys. Chem. B* **2001**, *105*, 6347. b) M. Adachi, Y. Murata, J. Liu, M. Sakamoto, F. Wang, *J. Am. Chem. Soc.* **2004**, *126*, 14 943. c) M. Thelakkat, C. Schmitz, H. W.Schmidt, *Adv. Mater.* **2002**, *14*, 577.
[7] a) G. Oskam, B. V. Bergeron, G. J. Meyer, P. C. Searson, *J. Phys. Chem. B* **2001**, *105*, 6867. b) H. Nusbaumer, S. M. Zakeeruddin, J.-E. Moser, M. Grätzel, *Chem. Eur. J.* **2003**, *9*, 3756.
[8] a) M. Adachi, Y. Murata, J. Takao, J. Jiu, M. Sakamoto, F. Wang, *J. Am. Chem. Soc.* **2004**, *126*, 14 943. b) S. Ushiroda, N. Ruzycki, Y. Lu, M. T. Spitler, B. A. Parkinson, *J. Am. Chem. Soc.* **2005**, *127*, 5158.
[9] T. Horiuchi, H. Miura, K. Sumioka, S. Uchida, *J. Am. Chem. Soc.* **2004**, *126*, 12 218.
[10] a) M. K. Nazeeruddin, P. Pechy, T. Renouard, S. M. Zakeeruddin, R. Humphry-Baker, P. Liska, L. Cevey, E. Costa, V. Shklover, L. Spiccia, G. B. Deacon, C. A. Bignozzi, M. Grätzel, *J. Am. Chem. Soc.* **2001**, *123*, 1613, b) M. Grätzel, *Inorg. Chem.* **2005**, *44*, 6841. c) Z. S. Wang, T. Yamaguchi, H. Sugihara, H. Arakawa, *Langmuir* **2005**, *21*, 4272.
[11] P. Wang, S. M. Zakeeruddin, J. E. Moser, R. Humphry-Baker, P. Comte, V. Aranyos, A. Hagfeldt, M. K. Nazeeruddin, M. Grätzel, *Adv. Mater.* **2004**, *16*, 1806.
[12] M. K. Nazeeruddin, S. M. Zakeeruddin, K. Kalyanasundaram, *J. Phys. Chem.* **1993**, *97*, 9607.
[13] W. Wieczorek, P. Lipka, G. Zukowska, H. Wycislik, *J. Phys. Chem. B* **1998**, *102*, 6968.
[14] B. Wenger, M. Grätzel, J.-E. Moser, *J. Am. Chem. Soc.* **2005**, *127*, 12 150.
[15] J. B. Asbury, N. A. Anderson, E. Hao, X. Ai, T. Lian, *J. Phys. Chem. B* **2003**, *107*, 7376.
[16] P. Wang, S. M. Zakeeruddin, R. Humphry-Baker, J.-E. Moser, M. Grätzel, *Adv. Mater.* **2003**, *15*, 2101.
[17] J. Bisquert, *J. Phys. Chem. B* **2002**, *106*, 325.
[18] a) J. Bisquert, *Phys. Chem. Chem. Phys.* **2003**, *5*, 5360. b) J. van De Lagematt, N. G. Park, A. J. Frank, *J. Phys. Chem. B* **2000**, *104*, 2044. c) J. Bisquert, A. Zaban, M. Greenshtein, I. Mora-Sero, *J. Am. Chem. Soc.* **2004**, *126*, 13 550.
[19] F. Fabregat-Santiago, J. Bisquert, G. Garcia-Belmonte, G. Boschloo, A. Hagfeldt, *Sol. Energy Mater. Sol. Cells* **2005**, *87*, 117.
[20] Q. Wang, J.-E. Moser, M. Grätzel, *J. Phys. Chem. B* **2005**, *109*, 14 945.
[21] D. Kunag, P. Wang, S. Ito, S. M. Zakeerudddin, M. Grätzel, *J. Am. Chem. Soc.* **2006**, *128*, 7732.
[22] C. Lottner, K.-C. Bart, G. Bernhardt, H. Brunner, *J. Med. Chem.* **2002**, *45*, 2079.